Dyes and Pigments 92 (2011) 619–625

Contents lists available at ScienceDirect

Dyes and Pigments

journal homepage: www.elsevier.com/locate/dyepig

Seven-membered ring excited-state intramolecular proton-transfer in 2-benzamido-3- (pyridin-2-yl)acrylic acid

Zhao-Qi Guo [a,b], Wei-Qiang Chen [a], Xuan-Ming Duan [a,*]

[a] Laboratory of Organic NanoPhotonics and Key Laboratory of Functional Crystal and Laser Technology, Technical Institute of Physics and Chemistry, Chinese Academy of Sciences, Beijing 100190, China
[b] Graduate School of Chinese Academy of Sciences, No. 2, Beiyitiao, Zhongguancun Road, Haidian District, Beijing 100190, China

ARTICLE INFO

Article history:
Received 3 April 2011
Received in revised form
21 May 2011
Accepted 2 June 2011
Available online 22 June 2011

Keywords:
Excited-state intramolecular proton-transfer
Hydrogen bonding
Seven-membered ring
Dual emission
Solvent effect
Theoretical calculation

ABSTRACT

Hydrogen bonding compound (E)-2-benzamido-3-(pyridin-2-yl) acrylic acid (**1a**) was synthesized and characterized by ^{1}H NMR, FT-IR, and X-ray diffraction analysis in comparison to its analog. These analyses show the existence of seven-membered ring intramolecular hydrogen bonding in **1a**. The hydrogen bonding results in the increasing of pK_a comparing to its analog. Further investigation on the photophysical properties of **1a** in selected solvents reveals that strong absorption appears at about 340 nm and dual emission at around 420 and 490 nm. The excited-state intramolecular proton-transfer in **1a** is very sensitive to solvent polarity and fluoride ion. Theoretical studies also give evidence of excited-state intramolecular proton-transfer with quite low energy barrier.

© 2011 Elsevier Ltd. All rights reserved.

1. Introduction

Proton transfer is one of the most fundamental reactions, and it is found ubiquitously in chemical and biological processes [1,2]. Various types of proton transfer have been reported in both the ground and excited states. Excited-state intramolecular proton-transfer (ESIPT) has received much attention because of the simplicity of its reaction pattern. The ESIPT system generally requires hydrogen bonding (H-bonding) formation between vicinal proton-donor groups and proton-acceptor groups. Upon photoexcitation, proton transfer from the donor to the acceptor moiety generates phototautomer fluorescence at low energy with an unusually large Stokes shift. Weller's pioneering work on salicylic acid and its derivatives led to an upsurge in research on ESIPT reactions [3]. Numerous ESIPT molecules have been strategically designed and synthesized to investigate the fundamental proton-transfer mechanism and/or to explore potential applications of ESIPT molecules in UV stabilizers [4,5], tunable lasers [6], optical switching [7], data storage [8], fluorescent labeling [9], and as ion probes [10,11].

In terms of hydrogen-bonding structure, ESIPT molecules can be classified by the atom numbers involved in the hydrogen-bonded ring: (a) five-membered-ring (5-MR) hydrogen-bonding systems, *e.g.* 8-hydroxyquinoline [12], 2-hydroxy-4,5-naphthotropone [13], 3-hydroxyflavone [14], 2-pyridylpyrazole [15], and 3-hydroxychromones [16]; (b) six-membered-ring (6-MR) hydrogen-bonding systems, *e.g.* salicylic acid and its associated derivatives [3,17–20], 5-hydroxyflavone [21], 1,5-dihydroxyxanthraquinone [22], 1-(acy1amino) anthraquinone [23], 2-hydroxy-1-naphthaldehyde [24], 2-(2′-hydroxyphenyl)benzoxazole (or benzothiazole) [25–28], and 9-hydroxyphenalenone [28]; and (c) seven-membered-ring (7-MR) hydrogen-bonding systems, e.g. 4-(2-hydroxy-benzylidene)-1,2-dimethyl-1*H*-imidazol-5(4*H*)-one (*o*-HBDI), which is akin to the core chromophore of green fluorescent protein [29]. In the studied molecules, the pyridine moiety is one of the most important proton acceptors, and its derivatives have been extensively investigated as intramolecular proton-transfer systems with hydroxyl and amino groups as proton donors [30–33]. Although intermolecular proton-transfer exists between pyridine and aliphatic acids, no intramolecular proton-transfer was observed in picolinic acid, which can be verified from the appearance of the chemical shift of the carboxylic OH at 10.03 ppm [34].

In this paper, we designed and synthesized an intramolecular 7-MR hydrogen-bonding system, (E)-2-benzamido-3-(pyridin-2-yl)

* Corresponding author. Tel.: +86 10 8254 3596; fax: +86 10 8254 3597.
E-mail address: xmduan@mail.ipc.ac.cn (X.-M. Duan).

0143-7208/$ – see front matter © 2011 Elsevier Ltd. All rights reserved.
doi:10.1016/j.dyepig.2011.06.004

acrylic acid (**1a**, Scheme 1), in which the carboxylic OH acts as a proton donor, the pyridine acts as a proton acceptor, and the benzamido moiety is introduced to keep the carboxylic acid moiety in the *cis* position of the pyridine. The *cis* form positions the donor close to the acceptor and favors the formation of intramolecular H-bonding between the pyridyl and hydroxyl groups. The intramolecular 7-MR H-bonding in **1a** was characterized by ^{1}H NMR, FT-IR, and single crystal X-ray diffraction. Its photophysical properties were investigated to understand the ESIPT process in **1a** compared with those of its analog 2-benzamido-3-(pyridin-4-yl) acrylic acid (**1b**). Furthermore, the energy barrier of ESIPT was investigated using theoretical studies.

2. Experimental details

2.1. Measurements

^{1}H NMR spectra were recorded on a Bruker Avance II-400 spectrometer (Bruker Corporation), in $CDCl_3$ and DMSO-d_6 with TMS as internal standard. The fine splitting of pyridyl or phenyl ring patterns was ignored and the signals reported as simple doublets, with *J* values referring to the two most intense peaks. Elemental analyses were performed on FlashEA 1112 (Thermo Fisher Scientific Inc.). Mass spectra were measured on a Waters GCT Premier spectrometer (Waters Corporation). The absorption spectra were recorded on a Shimadzu UV-2550 UV–visible spectrophotometer (Shimadzu, Kyoto, Japan), and the fluorescence spectra were using a Hitachi F-4500 fluorescence spectrophotometer (Hitachi, Tokyo, Japan). IR spectra were measured on a Varian Excalibur 3100 FT-IR spectrometer (Varian). X-ray diffraction data were collected on a Bruker Apex II CCD diffractometer with Mo K_α radiation ($\lambda = 0.71073$ Å) at room temperature.

2.2. Materials

Pyridine-2-carbaldehyde, pyridine-4-carbaldehyde and tetrabutylammonium fluoride (TBAF) were purchased from J&K Chemicals Ltd, Beijing, China. Benzoyl chloride, glycine, sodium hydroxide (NaOH) and sodium bicarbonate ($NaHCO_3$), chloroform ($CHCl_3$), acetic anhydride (Ac_2O) were purchased from the Beijing Chemical Reagent Company. Ethanol (EtOH), methyltetrahydrofuran (MeTHF), acetonitrile (MeCN), and *n*-hexane (Hex, spectroscopic grade; Acros) were used as supplied. Ultrapure water (H_2O) was obtained from a Milli-Q Plus water purification system (Millipore) and had a resistivity of 18.2 MΩ. Compounds **1a**–**b** were synthesized using a previously reported procedure [35,36].

Data for **1a**: ^{1}H NMR (400 MHz, DMSO-d_6, δ) 7.63 (4 H, m), 7.81 (1 H, d, $J = 8$ Hz), 7.91 (2 H, d, $J = 7.8$ Hz), 8.12 (1 H, s), 8.20 (1 H, td, $J_1 = 7.8$ Hz, $J_2 = 1.6$ Hz), 8.75 (1 H, d, $J = 4.6$ Hz), 10.01 (1 H, s), 19.85 (1 H, bs). ^{1}H NMR (400 MHz, $CDCl_3$, δ) 7.44 (1 H, dd, $J_1 = 6.6$ Hz, $J_2 = 6.3$ Hz), 7.51 (2 H, t, $J = 7.5$ Hz), 7.58 (1 H, t, $J = 7.2$ Hz), 7.63 (1 H, d, $J = 8.0$ Hz), 7.95 (2 H, d, $J = 7.5$ Hz), 8.04 (1 H, t, $J = 8.0$ Hz), 8.46 (1 H, dd, $J_1 = 4.8$ Hz, $J_2 = 2.4$ Hz), 8.71 (1 H, s), 9.96 (1 H, s), 21.61 (1 H, s). ^{13}C NMR (100 MHz, $CDCl_3$, δ) 113.0, 123.0, 127.3 (2C), 127.8, 129.0 (2C), 132.5, 134.3, 136.6, 141.7, 142.4, 150.8, 165.0, 166.2. MS (*m*/*z*): 250.0656 (100%, $[M\text{-}H_2O]^+$). Elemental analysis: Calcd.: 67.16% C, 4.51% H, 10.44% N; observed: 67.02% C, 4.58% H, 10.20% N. m.p. 176–178 °C.

Data for **1b**: ^{1}H NMR (400 MHz, DMSO-d_6, δ) 7.31 (1 H, s), 7.51 (4 H, m), 7.60 (1 H, t, $J = 7.4$ Hz), 7.96 (2 H, d, $J = 7.4$ Hz), 8.57 (2 H, d, $J = 6.2$ Hz), 10.11 (1 H, s), 13.20 (1 H, bs). m.p. 183–184 °C.

2.3. Theoretical approaches

The Gaussian 03 program [37] was used to perform *ab initio* calculations on the molecular structure. Geometry optimization for S_0 was carried out using density functional theory (DFT) methods [38], while the configuration interaction single (CIS) method [39] was employed to optimize the geometries for the excited states (S_1). The 6-31 + G(d,p) basis set was used for geometry optimization. Frequency calculations using the same methods as those for the geometry optimizations were performed for the obtained structures. One imaginary frequency indicated the existence of a transition state. Single-point energy calculations were performed at DFT level. Vertical electronic excitation energies were predicted using the TD-B3LYP/6-31 + G(d,p) method with the ground-state and excited-state optimized geometries, respectively.

3. Results and discussion

3.1. Intramolecular hydrogen bonding in the ground state

The intramolecular H-bonding in the ground state contributes to the changes in physicochemical properties and can be characterized by ^{1}H NMR and FT-IR. The physicochemical properties of **1a** are quite different from those of its analog **1b**. Compound **1a** is readily dissolved in $CHCl_3$ and MeCN, and is slightly soluble in water. **1b** is soluble in water, but poorly soluble in $CHCl_3$ and other non-polar solvents. In the ^{1}H NMR spectra, the chemical shift of the acrylic C=C–H group in **1a** is 8.12 ppm in DMSO-d_6, 0.81 ppm downfield of the acrylic group in **1b**. This indicates a strong electron-withdrawing group connected to the acrylic C=C and conversion of the pyridine moiety to pyridinium. The chemical shift of the carboxyl proton for **1a** appears as a broad peak at 19.85 ppm in DMSO-d_6, compared with 13.06 ppm for **1b**, 10.03 ppm for picolinic acid [34], and 8.39 ppm for the pyridinium proton in pyridinium chloride. This peak shifts to down filed 21.61 ppm in $CDCl_3$ as a sharp peak. These results strongly suggest that the carboxyl proton is involved in intramolecular H-bonding which is affected by solvents. In this intramolecular hydrogen-bonding system, the proton vibrates between the carboxylate COO^- anion and the pyridine N atom. This is totally different from the reported Z-form of this compound, which does not have intramolecular H-bonding [40].

IR spectra also give evidences of the intramolecular H-bonding in **1a**. The O–H stretching vibration of **1b** appears at ~3400 cm^{-1} (Fig. S1), but no such vibration is observed in the spectrum of **1a**. There are significant differences in the C=O stretching vibration frequencies for **1a** and **1b**. In both **1a** and **1b**, there are two carbon–oxygen double bonds: the amide C=O bond and the acrylic acid C=O bond. The C=O stretching vibrations of the amide and acrylic acid moieties for **1b** appear at 1665 cm^{-1} and 1724 cm^{-1}, respectively. In contrast, **1a** has only one C=O stretching vibration band, which appears at 1674 cm^{-1} and can be assigned to the amide C=O. The disappearance of acrylic acid C=O stretching vibration band at 1720 cm^{-1} indicates the presence of an acrylate anion structure in **1a**. These results show the existence of strong intramolecular H-bonding existing in **1a**, resulting in a zwitterionic form of **1a** in the solid state.

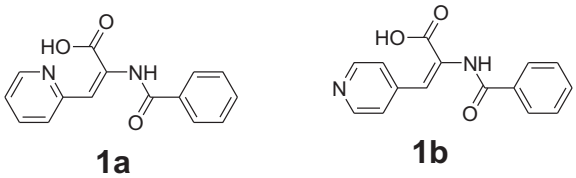

Scheme 1. The structures of **1a** and **1b**.

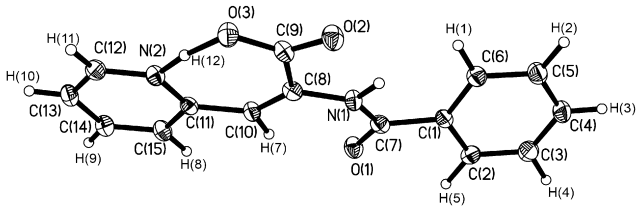

Fig. 1. Perspective view of **1a** showing the atom labeling schemes. Displacement ellipsoids of non-hydrogen atoms are at the 30% probability level.

The existence of strong H-bonding in the molecular structure of **1a** is further confirmed by single-crystal X-ray diffraction analysis. Recrystalization from a MeCN solution of **1a** by Hex diffusion produced crystals for single-crystal X-ray diffraction (CCDC reference number 687456) [41]. The structure of **1a** is orthorhombic, and its space group belongs to P_{212121}. The perspective view and packing of **1a** is illustrated in Fig. 1. There is H-bonding between the acrylate O(3) and the pyridine N(2) atoms; the distance between these two atoms is 2.483 Å, and the O(3)–H(12)–N(2) angle is 171.3°. Atoms C(7), C(15), N(1), N(2), O(1), and O(3) are involved in seven-membered-ring H-bonding in a plane forming a dihedral angle of 159.5° with the phenyl ring. The O(3)–H(12) distance is 1.345 Å (the theoretical distance is 0.920 Å for general carboxyl O-H), which is longer than the N(2)–H(12) distance of 1.145 Å (the general distance is 0.960 Å). The distance difference revealed that H(12) is closer to the pyridine N(2) than it is to the acrylate O(3). The O(2)–C(9) and O(3)–C(9) distances are 1.233 Å and 1.272 Å, respectively. These results show that H(12) is involved in a strong intramolecular H-bonding, N(2)–H(12)…O(3), in which the H(12) interaction with the pyridine N(2) is stronger than that with O(3). The carboxylic acid proton moves to the pyridine N atom, while an electron delocalizes across O(2), O(3), and C(9) to form two almost equivalent carbonyl groups. This is consistent with the disappearance of the C≡O stretching vibration bands at about 1720 cm^{-1} in the FT-IR spectrum. These results provide further evidence that compound **1a** exists mainly as a tautomeric form **1a**(NH) in the solid state (Scheme 2).

3.2. Excited-state intramolecular proton transfer

It has been reported that intramolecular proton-transfer is facilitated in the excited state if there is intramolecular H-bonding between two moieties in the ground state [42]. ESIPT in **1a** results in the formation of its two tautomeric forms in the excited state. These tautomeric forms exhibit different photophysical properties.

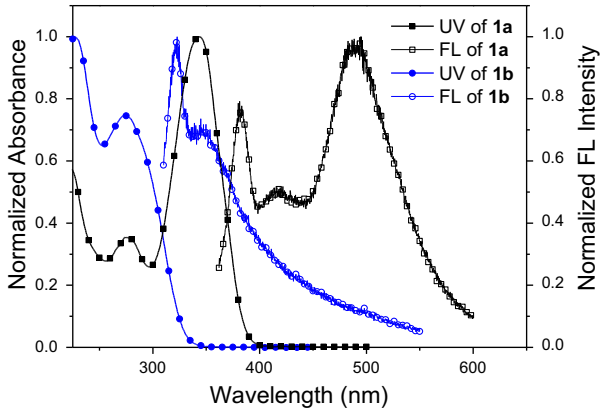

Fig. 2. Normalized UV–visible absorption and fluorescence spectra of **1a** and **1b** in MeCN (1.0×10^{-5} M). The excitation wavelength is 343 nm for **1a** and 275 nm for **1b**, the excitation and emission slits are 10 nm.

3.2.1. Absorption and fluorescence spectra

The normalized absorption and fluorescence spectra of **1a** and **1b** in MeCN are shown in Fig. 2. Compound **1b** in MeCN (1.0×10^{-5} M) exhibits a lowest lying transition maximum at 274 nm. The absorption extinction coefficient (ε) is 1.25×10^4 M^{-1} cm^{-1}, which shows S_0–S_1 is π–π* transition. In contrast, the UV absorption spectrum of **1a** in MeCN exhibits not only a transition at 274 nm with $\varepsilon = 0.94 \times 10^4$ M^{-1} cm^{-1}, but also a lowest lying transition maximum at 343 nm with $\varepsilon = 2.67 \times 10^4$ M^{-1} cm^{-1}. The absorption band at 274 nm can be assigned to the π–π* transition from twisted pyridyl, benzoyl amide, and acrylate moieties. Because the pyridine ring and the acrylate moiety in **1a** are fixed in a plane by a 7-MR H-bonding, the π-conjugation system is enlarged in **1a**, the band at 343 nm can be assigned to the π–π* transition from the conjugated pyridyl and acrylate moieties. The photophysical data of **1a** and **1b** are listed in Table 1.

Excited at 275 nm, **1b** in MeCN depicts two emission bands: one very sharp peak at 321 nm with a full width at half maximum (FWHM) of 10 nm and another shoulder broad peak at 346 nm. In comparison, **1a** shows three peaks: one sharp peak at 382 nm with a FWHM of 10 nm, one peak at 420 nm and another at 490 nm. After calculation, we found the peak at 321 nm for **1b** and 382 nm for **1a** in emission spectra are Raman scattering arising from C–H vibration since very weak fluorescence. These two peaks shift with the excitation wavelength. The emission spectra at 77 K also prove these peaks are from Raman scattering (Fig. 6). Thus, the emission band at 420 nm may be the normal form emission of **1a**. The peak at 490 nm shows abnormal large Stokes shift of 8700 cm^{-1}, which may be assigned to the ESIPT emission.

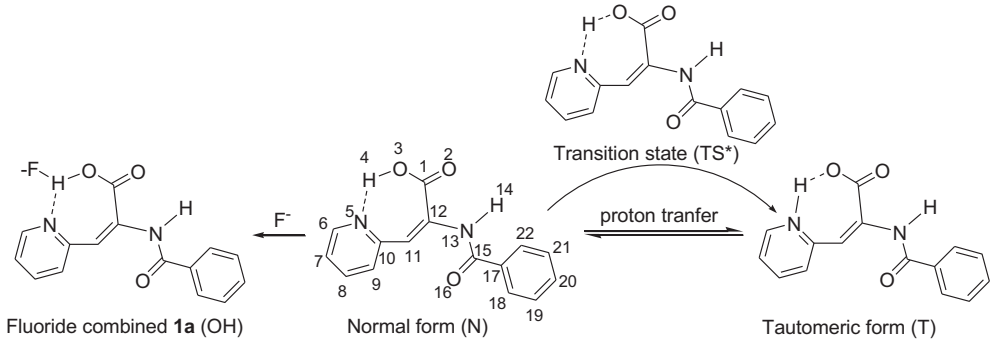

Scheme 2. Geometries of tautomeric forms of **1a**, along with atom numbering.

Table 1
Photophysical data of **1a** and **1b** in selected solvents.

	Solvents	λ_{ab}/nm (ε/$M^{-1}cm^{-1}$)[a]	λ_{em}/nm[b]	Φ[c]
1a	H_2O	276 (13,500), 333(31,600)	420, 490	0.0012
	EtOH	282(12,500), 336(31,200)	420, 489 (298 K) 418 (77 K)	0.0016
	MeTHF	273(12,600) 339(40,100)	415, 490 (298 K) 410, 490 (77 K)	0.0039
	MeCN	274(12,700), 343(41,600)	420, 490	0.0014
	Hex	285(12,200), 343(38,300)	410, 500	0.0021
1b	MeCN	274 (12,500)	350	0.0021

[a] Absorption maximum and extinction coefficient.
[b] Emission peak excited at 343 nm for **1a** and 275 nm for **1b**.
[c] Fluorescence quantum yield using quinine sulfate in 1.0 N sulfuric acid ($\Phi = 0.51$) as reference standard [43].

In the buffer solution, the absorption maximum at 343 nm decreased and the absorption at 300 nm increased with pH value increasing, as shown in Fig. 3(a). The pK_a value of **1a** was determined as 6.0 ± 0.1 by using a reported method [44], which is larger than 4.25 for that of acrylic acid and less than 6.25 for pyridinium ion, respectively [45]. We further investigated influence of acid and base on **1a**'s absorption spectra. As showed in Fig. 3(b), the absorption maximum shifts to 310 nm when 5.0 equivalents NaOH are added to **1a** in MeCN. Accordingly, its fluorescence spectrum exhibits only one strong peak at 394 nm with 10-fold intensity. In this case, ESIPT is inhibited while the intramolecular H-bonding is broken by base. The emission of anion form **1a** must be similar to the normal emission of **1a** (420 nm). With addition of 5.0 equivalents TFA, the absorption maximum decreases slightly. However, the peak at 274 nm increases remarkably. The emission spectrum shows one peak at 466 nm. These results indicate interaction between TFA and pyridyl moiety of **1a** effecting the intramolecular H-bonding.

3.2.2. The effect of fluoride ion

In order to make clear assignment of emission peaks of **1a**, we further investigated the absorption and emission spectra of **1a** in MeCN with addition of TBAF. Since the fluoride ion will form strong H-bonding with O—H than nitrogen atom, the intramolecular H-bonding in **1a** will be destroyed. Therefore, the emission from tautomeric form of **1a** will disappear. As depicted in Fig. 4a, the absorption maximum of **1a** appears at 343 nm in MeCN without TBAF. It shifts to 318 nm with the 7.0 equivalents TBAF, which indicates the H-bonding broken and the fluoride-combined **1a**(OH) formed (The tautomeric forms of **1a** are shown in Scheme 2). With the excitation at 340 nm, **1a** in MeCN exhibits two peaks at ~420 and 490 nm (Fig. 4b). The excitation spectra monitored at 420 nm and 490 nm are identical (Fig. S2). This indicates that both emission bands originate from the same ground-state precursor. These results eliminate the possibility that the emission is a result of trace impurities. The intensity of emission peak at 490 nm decreased with the addition of TBAF and the peak disappeared with 2.0 equivalents TBAF. After adding 6.0 equivalent of TBAF, the emission peak at 420 nm also disappeared, a new peak at 402 nm appeared in the emission spectrum of **1a**, which is well in accordance with the emission at 402 nm of **1b** with 2.0 equivalents of TBAF. Hence we can confirm these emission bands unambiguously that the peak at 402 nm can be assigned to the emission from excited state of the fluoride-combined **1a**(OH), peak at 420 nm to that of normal form (N-form) and peak at 490 nm to that of the proton transfer tautomeric form (T-form), respectively. In ^{1}H NMR investigation, when one equivalent of TBAF is added to a $CDCl_3$ solution of **1a**, sharp peak at 21.61 ppm disappears (Fig. S5); meanwhile, proton signals of pyridine ring broaden and shift significantly. These results confirm the broken of intramolecular H-bonding and the variation of the absorption and emission spectra upon addition of TBAF. The intramolecular H-bonding in **1a** contributes to the two tautomer emissions in ACN solution.

3.2.3. Solvent effect

Furthermore, we investigated the solvent effect of **1a** (Fig. 5). The absorption maximum appears at 343 nm in MeCN, MeTHF and Hex, shifts to 336 nm in EtOH, and to 333 nm in water, indicating a blue shift of the absorption maximum with increasing solvent polarity. The photophysical data for **1a** and **1b** are summarized in Table 1.

With the excitation at 343 nm, **1a** shows clearly Raman scattering peak at around 382 nm in selected solvents (Fig. 5). Therefore clear dual emission was observed in emission spectra. These two emissions at around 420 (the F_1 band) and 490 nm (the F_2 band) varied in selected solvents. The ratios of the intensities of these two emission band (I_{F1}/I_{F2}) are 0.43 and 0.57 for **1a** in MeCN and EtOH, respectively. This ratio increased to 0.64 in MeTHF and 0.8 in Hex due to the decreasing emission at 490 nm (Fig. S3). These results show that the ratio increasing with the decreasing of solvent polarity. It means the higher solvent polarity may be in favor of the T-form emission of **1a** at 490 nm at 298 K. We noticed that the quantum yields of the T-form emission of 2-hydroxy-4,5-naphthotropone in EtOH and cyclohexane are 2.8×10^{-3} and 2.0×10^{-3} respectively. Jang et al proved it because intersystem crossing competes with proton transfer in cyclohexane but not EtOH solutions [13]. Thus, **1a** maybe undergoes similar deactivation process. The significant decrease of the T-form emission at 490 nm in water is due to polarity-induced fluorescence quenching and strong intermolecular H-bonding between **1a** and water.

As shown in Fig. 4, emission spectra of **1a** in MeTHF at 77 K also exhibits F_1 band at ~410 nm and F_2 band at ~490 nm, which are much stronger than those at 298 K. The ratio of I_{F1}/I_{F2} at 77 K became around 1. In a comparative study, **1b** only exhibits single

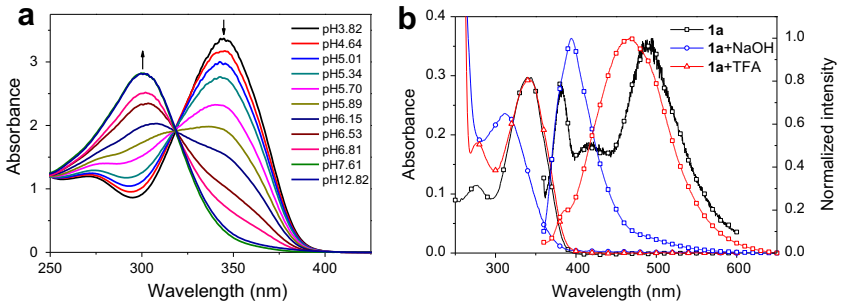

Fig. 3. a) UV spectra of **1a** at different pH values. b) The absorption and normalized fluorescence spectra of **1a** in MeCN with addition of acid and base.

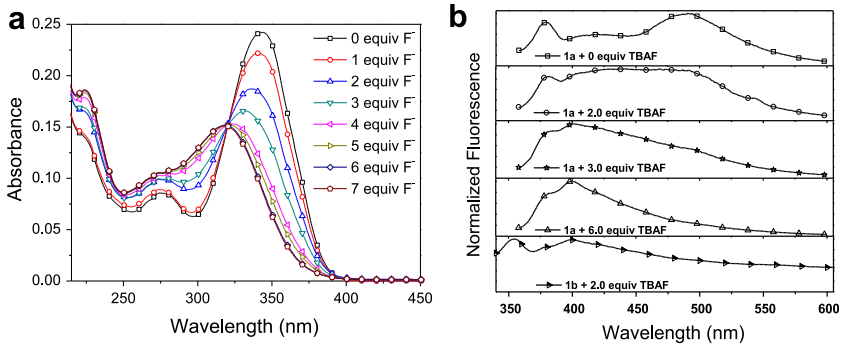

Fig. 4. Absorption (a, left) and Normalized fluorescence spectra (b, right) of **1a** in MeCN (1.0×10^{-5} M) with the addition of TBAF. The excitation wavelength is 340 nm for **1a** and 320 nm for **1b**, the excitation and emission slits are 10 nm.

emission at 365 nm at 77 K (Fig. 6), which is in accordance with the emission at 298 K in Fig. 1. However, **1a** shows only F_1 band at 418 nm in EtOH at 77 K. This is quite different from the room temperature situation. A similar case is 3-hydroxyflavone (3HF) which shows both normal and tautomer emission at 293 K in EtOH, however, predominantly normal emission at 77 K [14]. H-bonding perturbation by solvent molecules can prevent proton transfer in the excited state.

Using a 355 nm excitation beam from a YAG laser, the single-crystal also showed a major emission peak maximized at 490 nm and a shoulder peak at 420 nm (Fig. S4). The dual emission of **1a** at solid state is also in well accordance with the above results and gives further evidence to the ESIPT process.

3.3. Theoretical calculation

A computational approach was used to further understand the proton-transfer properties of **1a**. Geometries of normal form, transition state and tautomeric form of **1a**, along with atom numbering (some hydrogen atoms are omitted) are show in Scheme 2. Geometry optimization for the ground state normal form **1a(N)** based on the b3lyp/6-31 + G(d,p) theoretical level in the gas phase gives a structure for **1a(N)** similar to that obtained by single-crystal analysis. However, the hydrogen of the carboxyl group is close to the oxygen atom. The O(3)–H(4) distance is 1.031 Å, while the N(5)–H(4) length is 1.521 Å. The O(3)–H(4)–N(5) angle is 171.9° which is close to experimental data 171.3°. Optimization for the ground state tautomeric form **1a(T)** on the b3lyp/6-31 + G(d,p) level gives the same geometry as that of **1a(N)**. On removal of the hydrogen polarization function (6-31 + G(d)), as reported elsewhere [46], the optimized geometry of **1a(T)** still converged to that of **1a(N)**. These results indicate that **1a(T)** is very unstable in the ground state in the gas phase. This indicates that reverse intramolecular proton-transfer from **1a(T)** to **1a(N)** is barrierless. On the basis of time-dependent DFT, the $S_0 \rightarrow S_1$ transition is calculated to be 3.64 eV (341 nm, HOMO → LUMO, $f = 0.7401$) and 4.28 eV (290 nm, HOMO → LUMO + 1, $f = 0.0862$). These results correlate

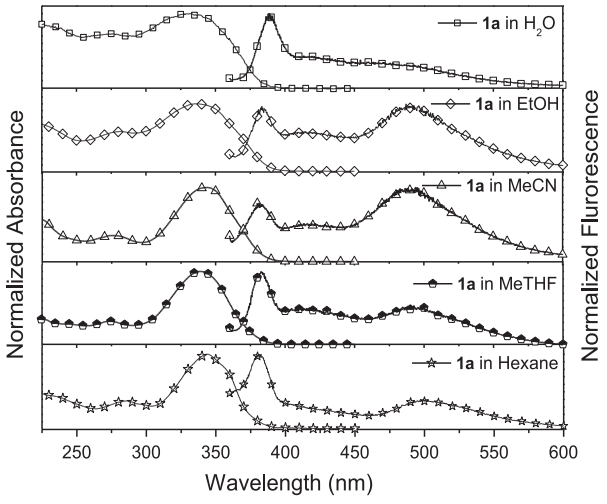

Fig. 5. Normalized UV–visible absorption and fluorescence spectra of **1a** in selected solvents (1.0×10^{-5} M).

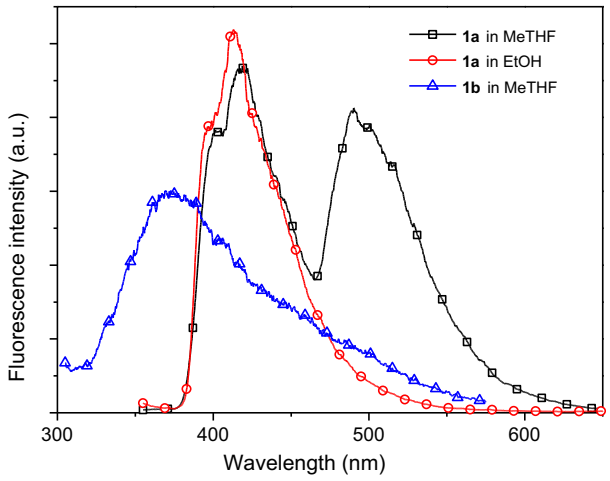

Fig. 6. Emission spectra of **1a** ($\lambda_{ex} = 343$ nm) and **1b** ($\lambda_{ex} = 275$ nm) in MeTHF and EtOH at 77 K.

Table 2
Main geometrical parameters (bond lengths and angles in angstroms and degrees, respectively) for the four stationary points (N, N*, TS*, T*) of **1a**.

	N (S_0)	N* (S_1)	TS* (S_1)	T* (S_1)
O_3–H_4	1.031	0.965	1.230	1.635
N_5–H_4	1.521	1.795	1.203	1.049
O_3–N_5	2.546	2.723	2.419	2.643
C_1–O_2	1.218	1.201	1.212	1.215
C_1–O_3	1.307	1.308	1.261	1.251
$\angle O_3$–H_4–N_5	171.9	160.2	167.7	159.4
N_{13}–H_{14}	1.016	1.000	1.003	0.999
O_2–H_{14}	1.937	2.046	1.948	2.165
$\angle O_2$–H_{14}–N_{15}	114.9	110.5	114.2	109.1
ΔE	0.87 kcal/mol			
ΔE_d	3.97 kcal/mol			

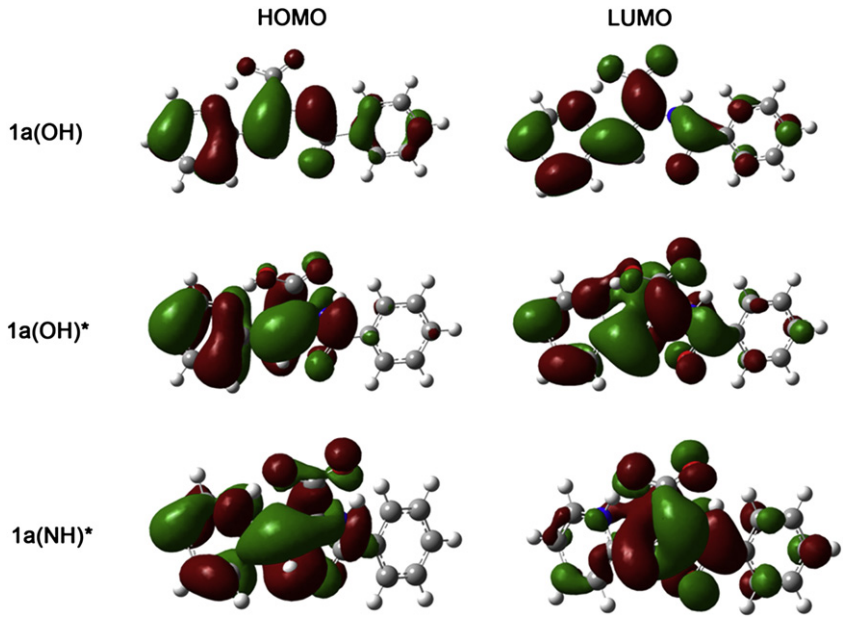

Fig. 7. The distribution patterns of HOMOs and LUMOs for **1a** (OH), **1a**(N)*, and **1a**(T)*.

well with the absorption bands at 343 nm and 274 nm, and with the excitation spectra of **1a**. The excited-state geometries of the normal form **1a(N)*** (where * denotes an electronically excited state), the tautomeric form **1a(T)***, and the transition state (TS*) were optimized based on the CIS/6-31 + G(d,p) level. The energy of **1a(T)*** is only 0.87 kcal mol^{-1} higher than that of **1a(N)***. The direct energy barrier for excited-state proton transfer is 3.97 kcal mol^{-1}. Such a low energy barrier is very easy to overcome. However, we observed quite weak fluorescence of both normal and tautomer emission. It means intersystem crossing is the major relaxation process of excited **1a**.

Furthermore, we compare geometrical parameters of the four stationary points. The bond lengths and angles for the four stationary points are listed in Table 2. Comparing the geometrical parameters involved in the intramolecular H-bonding of N*, TS* and T*, we can found that bond lengths of O_3—H_4 and N_5—H_4 are almost equal at TS* state. Other difference in the geometries of the transition states is the decrease in the interatomic distances between O_3—N_5 and the increase of the O_3—H_4—N_5 angle. The decreasing H-bonding strength and increasing of the O_3—H_4—N_5 angle in TS* will facilitate intramolecular proton transfer.

Frontier molecular orbital (FMO) analysis shows clear excited-state proton transfer features. As depicted in Fig. 7, the HOMO and LUMO distribution patterns in S_0 for **1a(N)** are similar. The excitation of the electron from the HOMO to the LUMO leads to small change in the electron density in S_1 for **1a(N)**. However, clear evidence of a charge transfer character can be observed from the FMOs of **1a(T)***. The electronic density flows mainly from the pyridine ring to the acrylic group, and extends to the benzene ring. The FMO distribution patterns in the S_1 state for **1a(N)*** and **1a(T)*** suggest a stronger charge-transfer character for **1a(T)*** than for **1a(N)***.

4. Conclusions

Molecule **1a** possesses a strong seven-membered ring intramolecular H-bonding and shows quite different physicochemical properties, such as solubility and pK_a, comparing with its analog **1b**. The π-conjugation between pyridyl and acrylate moieties is extended by intramolecular H-bonding leading to a strong absorption at about 340 nm. Intramolecular proton transfer facilitates in the excited state, resulting in dual emission at around 420 nm and 490 nm in MeCN. The tautomer emission at 490 nm is sensitive to solvent polarity, fluoride ion and base. The ratios of I_{F1}/I_{F2} show a rising tendency as solvents polarity increasing indicating intersystem crossing competing with proton transfer in low polarity solvents. And intersystem crossing is the major relaxation process of excited **1a** which is reasonable for low fluorescence quantum yield. Theoretical calculations show that the energy difference between **1a(N)*** and **1a(T)*** is 0.87 kcal mol^{-1} and proton transfer barrier is 3.97 *k*cal mol^{-1} in the excited state. As the photophysical properties of **1a** are sensitive to solvent polarity, fluoride ion and base, it gives a guide for design sensors based on ESIPT.

Acknowledgements

This work was supported financially supported by the National Natural Science Foundation of China (No. 50773091), the National Basic Research Program of China (No. 2010CB934103), the International Communication and Cooperation Project (2008DFA02050, 2010DFA01180) and the CREST Project of the Japan Science and Technology Agency (JST).

Appendix. Supplementary data

Supplementary data associated with this article can be found in the online version, at doi:10.1016/j.dyepig.2011.06.004.

References

[1] Jeffery GA, Saenger W. Hydrogen bonding in biological structures. New York: Springer-Verlag; 1994.
[2] Hibbert F. Mechanisms of proton transfer between oxygen and nitrogen acids and bases in aqueous solution. Adv Phys Org Chem 1987;22:113–212.
[3] Weller A. Innermolekularer protonenubergang im angeregten zustand. Z Electrochem 1956;60:1144–7.
[4] Catalan J, Fabero F, Guijarro MS, Claramunt RM, Maria MDS, Focesfoces MD, et al. Photoinduced intramolecular proton-transfer as the mechanism of ultraviolet stabilizers – a reappraisal. J Am Chem Soc 1990;112:747–59.
[5] Heller HJ, Blattmann HR. Some aspects of stabilization of polymers against light. Pure Appl Chem 1973;36:141–62.

[6] Chou P, McMorrow D, Aartsma TJ, Kasha M. The proton-transfer laser – gain spectrum and amplification of spontaneous emission of 3-hydroxyflavone. J Phys Chem 1984;88:4596–9.
[7] Kuldova K, Corval A, Trommsdorff HP, Lehn JM. Photoinduced generation of long-lived proton transfer states: Photoinduced proton transfer from 2-(2′4′-dinitrobenzyl)pyridine to a proton cage, the [2.1.1] cryptand. J Phys Chem A 1997;101:6850–4.
[8] Nishiya T, Yamauchi S, Noboru Hirota MB, Hanazaki I. Fluorescence studies of the intramolecularly hydrogen-bonded molecules ortho-hydroxyacetophenone and salicylamide and related molecules. J Phys Chem 1986;90:5730–5.
[9] Shynkar VV, Klymchenko AS, Piemont E, Demchenko AP, Mely Y. Dynamics of intermolecular hydrogen bonds in the excited states of 4′-dialkylamino-3-hydroxyflavones. On the pathway to an ideal fluorescent hydrogen bonding sensor. J Phys Chem A 2004;108:8151–9.
[10] Guo ZQ, Chen WQ, Duan XM. Highly selective visual detection of Cu(II) utilizing intramolecular hydrogen bond-stabilized merocyanine in aqueous buffer solution. Org Lett 2010;12:2202–5.
[11] Bohne C, Ihmels H, Waidelich M, Chang YW. N-acylureido functionality as acceptor substituent in solvatochromic fluorescence probes: detection of carboxylic acids, alcohols, and fluoride ions. J Am Chem Soc 2005;127:17158–9.
[12] Bardez E, Devol I, Larrey B, Valeur B. Excited-state processes in 8-hydroxyquinoline: photoinduced tautomerization and solvation effects. J Phys Chem B 1997;101:7786–93.
[13] Jang DJ, Kelley DF. Time-resolved and steady-state fluorescence studies of the excited-state intramolecular proton-transfer and relaxation of 2-hydroxy-4,5-naphthotropone. J Phys Chem 1985;89:209–11.
[14] McMorrow D, Kasha M. Intramolecular excited-state proton-transfer in 3-hydroxyflavone – hydrogen-bonding solvent perturbations. J Phys Chem 1984;88:2235–43.
[15] Yu WS, Cheng CC, Cheng YM, Wu PC, Song YH, Chi Y, et al. Excited-state intramolecular proton transfer in five-membered hydrogen-bonding systems: 2-pyridyl pyrazoles. J Am Chem Soc 2003;125:10800–100801.
[16] McMorrow D, Kasha M. Proton-transfer spectroscopy of 3-hydroxychromones – extreme sensitivity to hydrogen-bonding perturbations. J Am Chem Soc 1983;105:5133–4.
[17] Heldt J, Gormin D, Kasha M. A comparative picosecond spectroscopic study of the competitive triple fluorescence of aminosalicylates and benzanilides. Chem Phys 1989;136:321–34.
[18] Lahmani F, ZehnackerRentien A. Effect of substitution on the photoinduced intramolecular proton transfer in salicylic acid. J Phys Chem A 1997;101:6141–7.
[19] Smith KK, Kaufmann KJ. Picosecond studies of intra-molecular proton-transfer. J Phys Chem 1978;82:2286–91.
[20] Rodriguez-Santiago L, Sodupe M, Oliva A, Bertran J. Hydrogen atom or proton transfer in neutral and single positive ions of salicylic acid and related compounds. J Am Chem Soc 1999;121:8882–90.
[21] Martinez ML, Studer SL, Chou PT. Direct evidence of the excited-state intramolecular proton-transfer in 5-hydroxyflavone. J Am Chem Soc 1991;113:5881–3.
[22] Vanbenthem MH, Gillispie GD. Intramolecular hydrogen-bonding. 4. Dual fluorescence and excited-state proton-transfer in 1,5-dihydroxyanthraquinone. J Phys Chem 1984;88:2954–60.
[23] Smith TP, Zaklika KA, Thakur K, Barbara PF. Excited-state intramolecular proton-transfer in 1-(acylamino)anthraquinones. J Am Chem Soc 1991;113:4035–6.
[24] Chowdhury P, Panja S, Chakravorti S. Excited state prototropic activities in 2-hydroxy 1-naphthaldehyde. J Phys Chem A 2003;107:83–90.
[25] Itoh M, Fujiwara Y. Transient absorption and 2-step laser excitation fluorescence studies of photoisomerization in 2-(2-hydroxyphenyl)- benzoxazole and 2-(2-hydroxyphenyl)benzothiazole. J Am Chem Soc 1985;107:1561–5.
[26] Frey W, Laermer F, Elsaesser T. Femtosecond studies of excited-state proton and deuterium transfer in benzothiazole compounds. J Phys Chem 1991;95:10391–5.
[27] Heller A, Williams DL. Intramolecular proton transfer reactions in excited fluorescent compounds. J Phys Chem 1970;74:4473–80.
[28] Barbara PF, Walsh PK, Brus LE. Picosecond kinetic and vibrationally resolved spectroscopic studies of intramolecular excited-state hydrogen-atom transfer. J Phys Chem 1989;93:29–34.
[29] Chen KY, Cheng YM, Lai CH, Hsu CC, Ho ML, Lee GH, et al. Ortho green fluorescence protein synthetic chromophore; excited-state intramolecular proton transfer via a seven-membered-ring hydrogen-bonding system. J Am Chem Soc 2007;129:4534–5.
[30] Basaric N, Wan P. Excited state proton transfer (ESPT) from phenol to nitrogen and carbon in (2-hydroxyphenyl) pyridines. Photochem Photobiol Sci 2006;5:656–64.
[31] Poor B, Michniewicz N, Kallay M, Buma WJ, Kubinyi M, Szemik-Hojniak A, et al. Femtosecond studies of charge-transfer mediated proton transfer in 2-butylamino-6-methyl-4-nitropyridine N-oxide. J Phys Chem A 2006;110:7086–91.
[32] De Klerk JS, Szemik-Hojniak A, Ariese F, Gooijer C. Intramolecular proton-transfer processes starting at higher excited states: a fluorescence study on 2-butylamino-6-methyl-4-nitropyridine N-oxide in nonpolar solutions. J Phys Chem A 2007;111:5828–32.
[33] Szemik-Hojniak A, Deperasinska I, Jerzykiewicz L, Sobota P, Hojniak M, Puszko A, et al. Crystal structure, spectroscopic, and theoretical investigations of excited-state proton transfer in the doubly hydrogen-bonded dimer of 2-butylamino-6-methyl-4-nitropyridine N-oxide. J Phys Chem A 2006;110:10690–8.
[34] Jiang N, Ragauskas AJ. Selective aerobic oxidation of activated alcohols into acids or aldehydes in ionic liquids. J Org Chem 2007;72:7030–3.
[35] Somerville AW, Davies SG. Syntheses from pyridine aldehydes—III. Tetrahedron 1969;25:1105–8.
[36] Griffith RK, Harwood HJ. Synthesis of polymer + copolymers of β-(3-pyridyl)-dl-alanine. J Org Chem 1964;29:2658–62.
[37] Frisch MJ, Trucks GW, Schlegel HB, Scuseria GE, Robb MA, Cheeseman JR, et al. Gaussian 03, Revision E.01. Wallingford CT: Gaussian, Inc.; 2004.
[38] Parr RG, Yang W. Density-functional theory of atoms and molecules. Oxford: Oxford University Press; 1989.
[39] Foresman JB, Head-Gordon M, Pople JA, Frisch MJ. Toward a systematic molecular orbital theory for excited states. J Phys Chem 1992;96:135–49.
[40] Cativiela C, Diaz de Villegas MD, Garcia JI, Mayoral JA, Melendez E. Synthesis of z-2-acetamido(benzamido)- 3-hetaryl-2-propenoic acids. Quim Ser C Quim Organ Bioquim 1985;81:56–61.
[41] In each case, a semi-empirical absorption correction was applied using SADABS and the SAINT program was used for integration of the diffraction profiles (Bruker AXS, SAINT Software Reference Manual, Madison, 1998). The structure was solved by direct methods using the SHELXS program of SHELXTL package and refined with SHELXL (Sheldrick, G.M. SHELXTL NT Version 5.1. Program for Solution and Refinement of Crystal Structures, University of Göttingen, Germany, 1997). The final refinement was performed by full-matrix least-squares methods on F2 with anisotropic thermal parameters for all non-H atoms. Generally, C-bound hydrogen atoms were located geometrically and refined as riding, whereas O- and N-bound hydrogen atoms were first determined in difference Fourier syntheses and then fixed at the calculated positions. Isotropic displacement parameters of hydrogen atoms were derived from their parent atoms.
[42] Bangal PR, Chakravorti S. Excited state proton transfer in indole-2-carboxylic acid and indole-5-carboxylic acid. J Phys Chem A 1999;103:8585–94.
[43] Demas JN, Crosby GA. The measurement of photoluminescence quantum yields. J Phys Chem 1971;75:991–1024.
[44] Albert A, Serjeant EP. The determination of ionization constants, a laboratory manual. London & New York: Chapman and Hall; 1984.
[45] Krishnamoorthy G, Dogra SK. Spectral characteristics of the various prototropic species of 2-(4′-N, N-dimethylaminophenyl) pyrido[3,4-d]imidazole. J Org Chem 1999;64:6566–74.
[46] Chen CL, Lin CW, Hsieh CC, Lai CH, Lee GH, Wang CC, et al. Dual excited-state intramolecular proton transfer reaction in 3-hydroxy-2-(pyridin-2-yl)-4H-chromen-4-one. J Phys Chem A 2009;113:205–14.